Solid Freeform Fabrication 2023: Proceedings of the 34th Annual International Solid Freeform Fabrication Symposium – An Additive Manufacturing Conference
Reviewed Paper

Toolpath planning approach for parts with multiple revolving features for wire arc additive manufacturing

Wei Sheng Lim and Gim Song Soh

Engineering Product Development, Singapore University of Technology and Design, Singapore 487372, Singapore

Abstract

In wire arc additive manufacturing, existing toolpath planner for complex 3D shapes such as propellers and turbines, with multiple revolving features radiating tend to utilize a cylindrical slicing approach. Such slicing approaches are highly customized, complex, and not readily available for printing such 3D shapes. In addition, such complicated motion planning requires coordination between the print head and substrate motion to be synchronized well which can be difficult to achieve. In this paper, we propose an alternative strategy using planar slicing and adaptive width contour-based toolpath planner. To achieve this, a two-step approach is proposed with the substrate and radiating elements treated as separate features. The substrate is printed with part of the revolving feature, providing a flat surface for the second step to print from. The approach is applied for a propeller over 0.7m in diameter where a 3D scan is done to compare with the part model.

Introduction

Wire arc additive manufacturing (WAAM) is a form of additive manufacturing utilizing wire based feedstock with heating provided by electric arcs. WAAM can print near net shape products, enhancing the material utilization rate, reducing the material input cost especially compared to using machining. High deposition rate of WAAM, typically from 1 kg/h to 4kg/h, makes it attractive to print large parts [1]. However, WAAM does suffer from poor dimensional accuracy and poor surface finish, requiring post processing.

In WAAM, parts are typically sliced into planar layers, from which toolpath for each layer is generated. Two common forms of toolpath strategies are zig-zag and contour. Zigzag toolpaths create a set of linear deposition lines along a main direction to fill the interior area. The toolpath is simple to generate but suffers from poor conformance to the outer contour which can result in overfill or underfill in parts of the exterior. Contour toolpath instead generates deposition lines by offsetting from the outer contours, allowing high conformance to the outer shape but the discrete nature of the bead cases interior voids to form. Such voids are undesirable as are potential sources of failure which can weaken the structure. Adaptive width contour paths vary the process parameter and thus the bead width along the deposition path. This overcomes the discrete nature of the beads in traditional contour toolpath, reducing void formation while allowing conformation to the outer contour demonstrated in [2], [3]. Elkhouly et al. [4] have applied adaptive bead width to a hybrid WAAM with subtractive and additive processes to build a solid propeller blade, demonstrating the ability of adaptive bead width toolpath in printing complex shapes. However, further work is required to extend the printing from a single blade on a flat substrate to a propeller.

Using WAAM to print parts with multiple revolving features can be challenging when the part gets complex. These set of parts contains a central body form which a set of separate features, referred to as revolving features, radiate outwards. Each revolving feature is connected to the central body and radiates outwards with no intersection with other revolving features. Examples of such parts include propellers, turbines, impellers, pipe joints and helical gear. When such parts come with complex revolving features, it can be challenging to pick a single part orientation to eliminate overhang and thus eliminate support structure. Cylindrical slicing has been proposed by He et al. [5] and Dharmawan et al. [6] with the slices growing radially outwards to slice the revolving feature, taking advantage of how the revolved features extend outwards radially. However, traditional toolpath planning algorithms rely on planar slices and modification is required to consider the additional dimension affecting the contour offset algorithm. Such a change to the algorithm, would also require additional study to ensure the robustness. Alternatively, the cylindrical slices can be transformed and mapped to planar layers where traditional planar toolpath algorithm can be utilized such as in [7], [8], [9]. After toolpath generation, the toolpaths are transformed back to the original space, resulting in a cylindrical path. Since traditional bead modelling experiments are done on a flat substrate, a study is required to understand and map the bead parameters to the welding parameters for curved surfaces. This is to ensure an accurate model of bead and weld parameters to enable accurate adaptive bead width toolpath.

Multi-directional printing approach has been explored by various groups [10] [11] and can be seen as a middle ground where a part is separated into sub-volumes. Each sub-volume is sliced and printed with traditional planar algorithms with independent directions. This allows the print direction for each sub-volume to be optimized to reduce overhang regions. Through the use of planar slicing, adaptive bead width can then be applied to print each sub-volume. This allows us to rotate the part to print each revolving feature in a method similar to [4], enabling the entire part with revolving feature to be printed on a single system. This allows the interleaving of the print and cool down time between multiple revolving features, potentially reducing overall print time.
In this paper, the approach taken is described, along with the computations to support the implementation. The approach is then applied to print a propeller with a diameter exceeding 0.7m where a comparison to the input model is made.

Methods

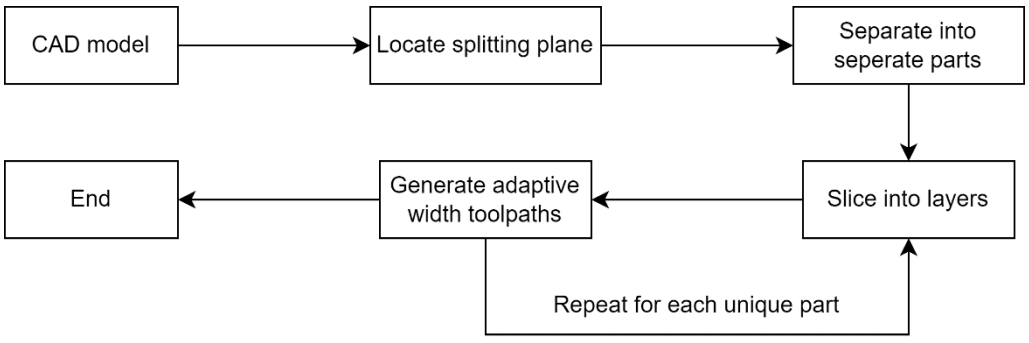

Fig. 1: Multi directional toolpath generation steps

Starting from the CAD model, the splitting planes need to be located, either manually or via an algorithm. For parts with revolving features, the splitting plane would be tangent to a cylinder or cone, concentric to the axis of revolution. The part is then split into sub-volumes and

exported as individual parts. From here on, each unique part is processed independently, generating the slices and toolpath in a traditional planar method. In parts with revolving features, only a copy of the similar revolving features needs to be processed, saving time and computational effort. In the printing stage, the print is carried out in stages, starting from the central piece, followed by the revolving features which prints from the central piece. To ensure consistent bead dimensions, the printing is done with the welding torch aligned to gravity and perpendicular to the slice layer. This can be achieved by rotating the part before printing each sub-volume, using tools such as a rotary table.

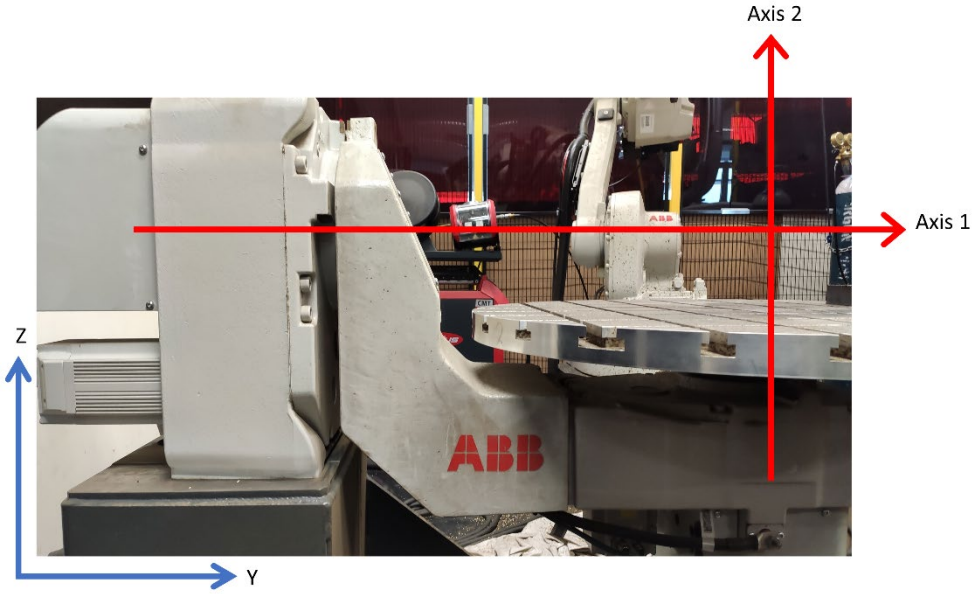

Fig. 2:Two-axis rotary table with axis in red and world frame in blue

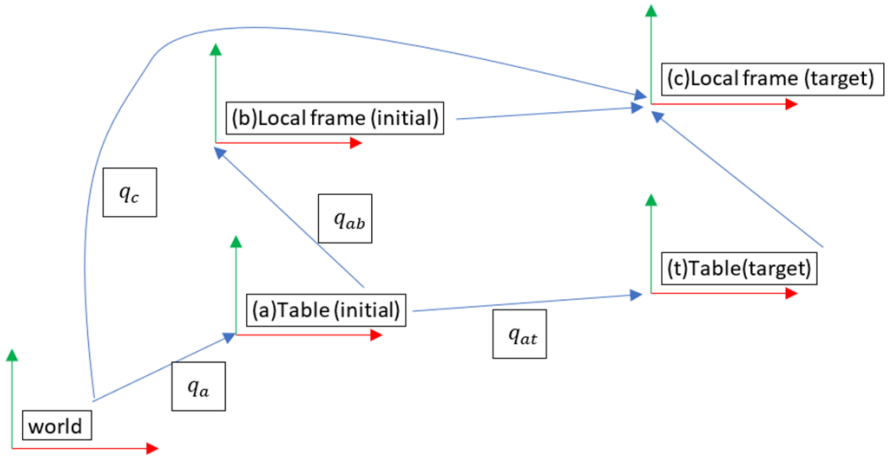

Fig. 3:Coordinate system for axis angle analysis

In the following, the required angle for each axis is computed for a two-axis rotary table depicted in Fig 2. A coordinate system in Fig. 3 is set up, with the table and local frame for printing in both initial and target orientation. The initial frames would be the orientation of the frames when the table is at zero degrees for both axis of the rotary table, while the target refers to the intended

orientation for printing. Quaternion is used to represent the initial orientation of the local frame with respect to the rotary table ($\boldsymbol{q}_{ab}$) and desired orientation of the local frame with respect to world frame ($\boldsymbol{q}_c$). It should be noted that multiple solutions can be achieved such that the welding torch is aligned as intended, for a two-axis rotary table, there are two solutions. The choice of x-y plane orientation in $\boldsymbol{q}_c$ would affect the final solution. With the orientation of the table with respect to world frame ($\boldsymbol{q}_a$), the orientations can be expressed by Equation (1). By making $\boldsymbol{q}_{at}$ the subject, we can get Equation (2) to obtain the required rotation in quaternions. The quaternion can then be expressed as a rotation matrix using Equation (3) which can be compared to the rotation matrix achieved by the desired system. In our setup, the rotary table has two axes of rotation possible with axis 1 aligned to the world y-axis and axis 2 aligned to the world z-axis. The rotation matrix can be formulated and expressed as in Equation (4) where the required angle for each axis can be computed by Equations (5) and (6) respectively. As a quick check, a nonzero value in $\boldsymbol{T}_{3,2}$ indicates that the rotary table is unable to achieve the desired rotation. For rotation with other setups, the same quaternion, q_{at}, can be utilized in inverse kinematics to obtain the required axes angles.

$$\boldsymbol{q}_c = \boldsymbol{q}_{ab}\boldsymbol{q}_{at}\boldsymbol{q}_a \tag{1}$$

$$\boldsymbol{q}_{at} = \boldsymbol{q}_a^*\boldsymbol{q}_c\boldsymbol{q}_{ab}^* \tag{2}$$

$$\boldsymbol{q} = \boldsymbol{q}_1 + \boldsymbol{q}_2 i + \boldsymbol{q}_3 j + \boldsymbol{q}_4 k = \begin{bmatrix} 2\boldsymbol{q}_1^2 - 1 + 2\boldsymbol{q}_2^2 & 2\boldsymbol{q}_2\boldsymbol{q}_3 + 2\boldsymbol{q}_1\boldsymbol{q}_4 & 2\boldsymbol{q}_2\boldsymbol{q}_4 - 2\boldsymbol{q}_1\boldsymbol{q}_3 \\ 2\boldsymbol{q}_2\boldsymbol{q}_3 - 2\boldsymbol{q}_1\boldsymbol{q}_4 & 2\boldsymbol{q}_1^2 - 1 + 2\boldsymbol{q}_3^2 & 2\boldsymbol{q}_3\boldsymbol{q}_4 + 2\boldsymbol{q}_1\boldsymbol{q}_2 \\ 2\boldsymbol{q}_2\boldsymbol{q}_4 + 2\boldsymbol{q}_1\boldsymbol{q}_3 & 2\boldsymbol{q}_3\boldsymbol{q}_4 - 2\boldsymbol{q}_1\boldsymbol{q}_b & 2\boldsymbol{q}_1^2 - 1 + 2\boldsymbol{q}_4^2 \end{bmatrix} \tag{3}$$

$$\boldsymbol{T}_{rotary} = \boldsymbol{R}z * \boldsymbol{R}y = \begin{bmatrix} \cos\theta_2 \cos\theta_1 & -sin\theta_2 & cos\theta_2 sin\theta_1 \\ sin\theta_2 cos\theta_1 & cos\theta_2 & sin\theta_2 sin\theta_1 \\ -sin\theta_1 & 0 & cos\theta_1 \end{bmatrix} \tag{4}$$

$$\theta_1 = \arcsin(-T_{3,1}) \tag{5}$$

$$\theta_2 = \arcsin(-T_{1,2}) \tag{6}$$

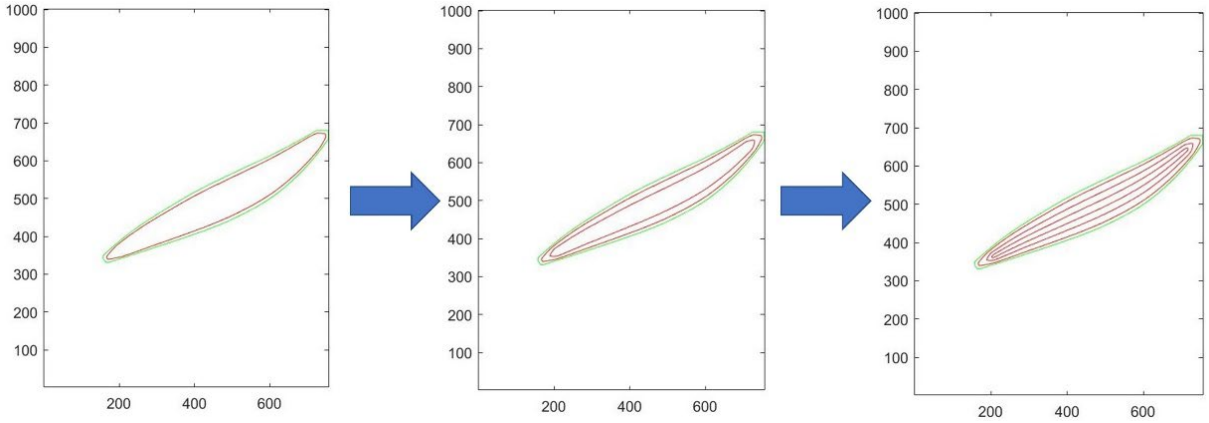

Fig. 4:Contour toolpath generation with variable width

For each slice, an adaptive bead width toolpath planning algorithm developed by Xiong et al. [3] is utilized to generate toolpaths. The toolpath is formed from two sets of contours, sliced layer contour ($\partial\Omega 1$) and the skeleton ($\partial\Omega 2$), also known as medial axis, which is generated by medial axis transformation from the sliced layer contour. To generate the toolpath, a signed

distance function is first applied to the two sets of contours, generating two distance fields using Equations (7) and (8). The distance field (Φ) is basically the distance between a point to the nearest element in the set of contours, with positive distance indicating points lying outside of the volume. A velocity field can then be computed using the difference between the two distance fields in Equation (9) with N being the number of contours and Δt as a virtual time interval. To get each toolpath, the contour is advanced towards the medial axis with the velocity field where thicker sections have higher velocity and thus wider beads and vice versa as seen in Fig 4. This is repeated until reaching the intended toolpath count which can be determined from the widest bead printable and the widest section of the part. Lastly, the bead width for each section obtained from obtained with Equation (10) is used to map to the printing parameters, wire feed speed and torch travel speed. The map is determined with a gaussian process regression and a series of single bead experiments, with further information from [3].

$$\Phi(\mathrm{p}) = \begin{cases} -d(p) & \text{if } p \in \Omega \\ 0 & \text{if } p \in \delta\Omega \\ d(p) & \text{if } p \notin \Omega \end{cases} \tag{7}$$

$$d(p) = \min(|p - p_i|) \text{ for all } p_i \in \delta\Omega \tag{8}$$

$$v(\Omega) = \big(\Phi(\partial\Omega 1) - \Phi(\partial\Omega 2)\big)/(N\Delta t) \tag{9}$$

$$w(c) = -v(c)\Delta t \tag{10}$$

Print setup and results

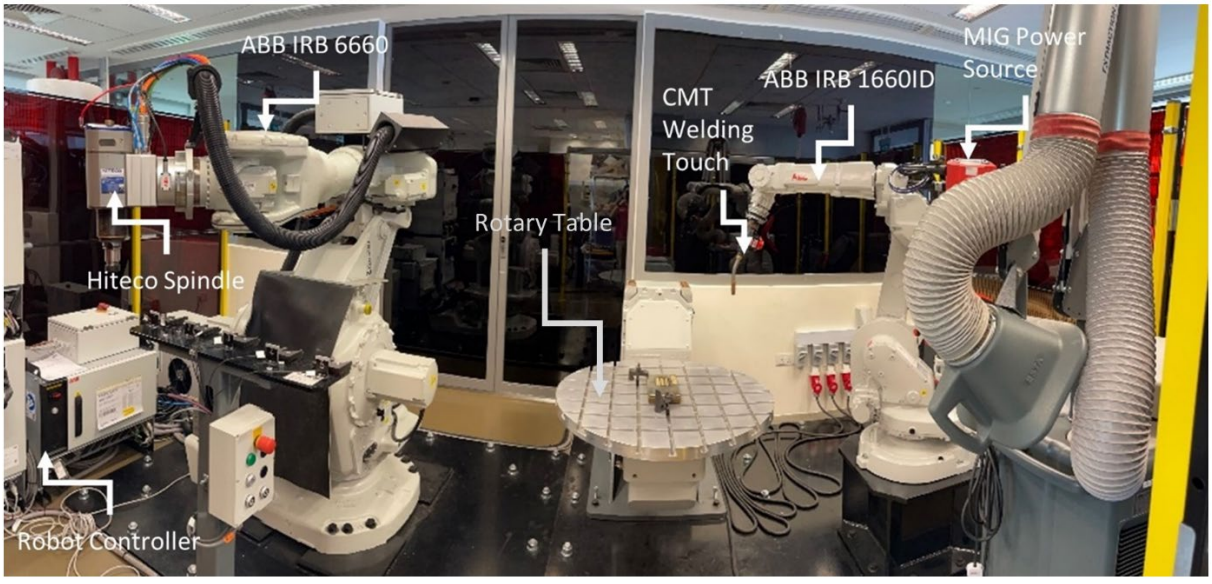

Fig. 5: Wire Arc Additive manufacturing system with two-axis rotary table

To verify the approach, a hybrid WAAM system is selected to implement the approach to print a propeller. Additive capability is provided by the welding torch (Fronius WF 60i Robacta Drive) held by a robotic arm (ABB IRB 1660ID) with a welding power source (Fronius TPS 400i). powering the torch. A secondary robotic arm manipulator (ABB IRB 6660) holds a spindle (Hiteco PX-2 20/10 24) for subtractive capability. The subtractive capability is useful to control error

accumulation during the printing process to prevent undesirable uneven layer height. The worktable is a rotary table, providing two additional degrees of freedom, allowing the part to be orientated as required. The feedstock chosen is AMPCOTRODE 46 nickel aluminum bronze, a material commonly used for propellers.

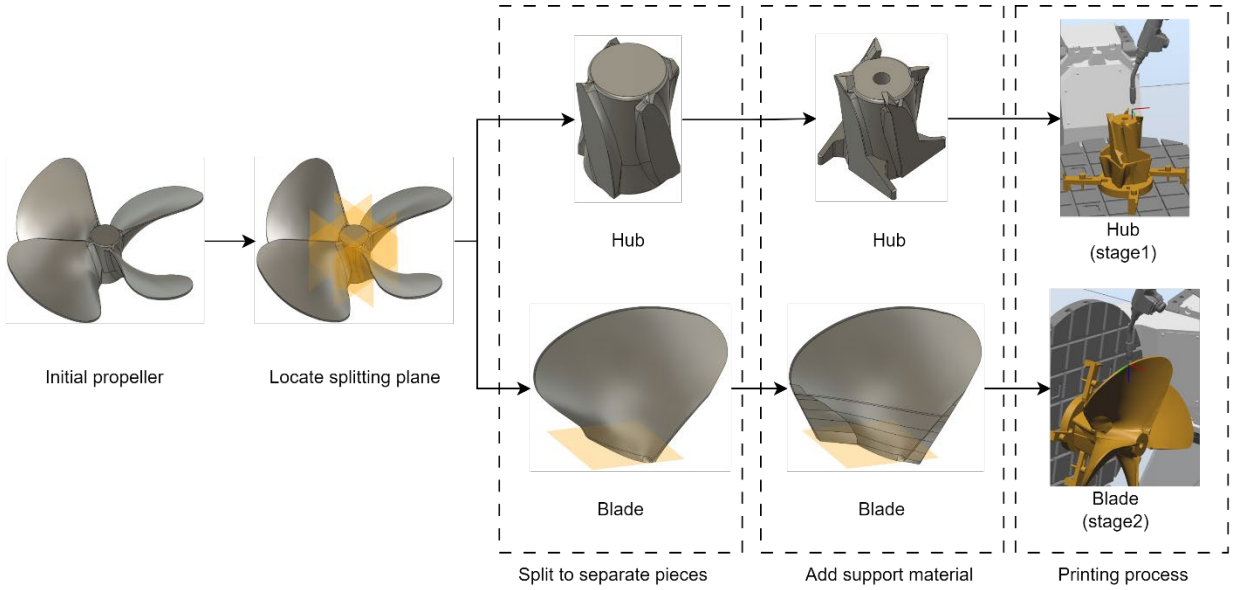

Fig. 6:Stages and steps to print a propeller with multi-directional printing

Table I

VOLUMES OF SUB-VOLUMES

Sub-volume	Original Volume (mm^3)	Volume with support (mm^3)	Difference(mm^3)
Hub	1.885×10^6	2.017×10^6	0.132×10^6 (7.00%)
Blade[a]	1.350×10^6	1.459×10^6	0.109×10^6 (8.07%)
Total[b]	7.285×10^6	7.853×10^6	0.568×10^6 (7.80%)

[a] Single blade only

[b] Consist of a hub and four blades

The propeller is sliced and separated into two unique parts, the hub and blade, where four copies of the blade are printed to achieve the final four bladed propeller. The blade could be further broken down into further sub-volumes with differing print direction to overcome overhang while keeping each piece vertical at each printing step. However, WAAM produces parts that are anisotropic, where the strength is dependent on the print direction. By using a single print direction for the blade, the strength variation along the blade can be simplified. In this case, support structure in the form of additional material is added to reduce overhang after splitting into separate parts and before slicing as shown in Fig. 6. Comparing the initial and modified models, we find that the support has added an additional 7.8% volume detailed in Table 1, which was deemed as an acceptable trade-off. Printing is carried out in two stages, with the central piece, a hub, being printed first, forming the substrate of the second stage. The second stage is where all four blades are printed at the same time in an alternating pattern. Such an approach has been shown to reduce warpage by balancing the stress at opposites as shown by [12]. Printing all four blades together

can also reduce the overall print time by interleaving the cooldown time and print time of the different blades together.

Fig. 7:Propeller printed using multi directional printing approach

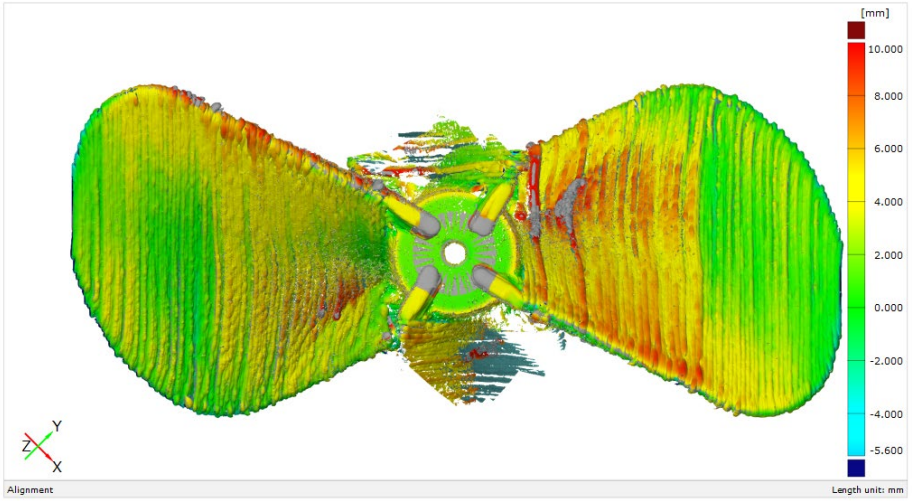

Fig. 8: Top view of scan for opposing propeller blades

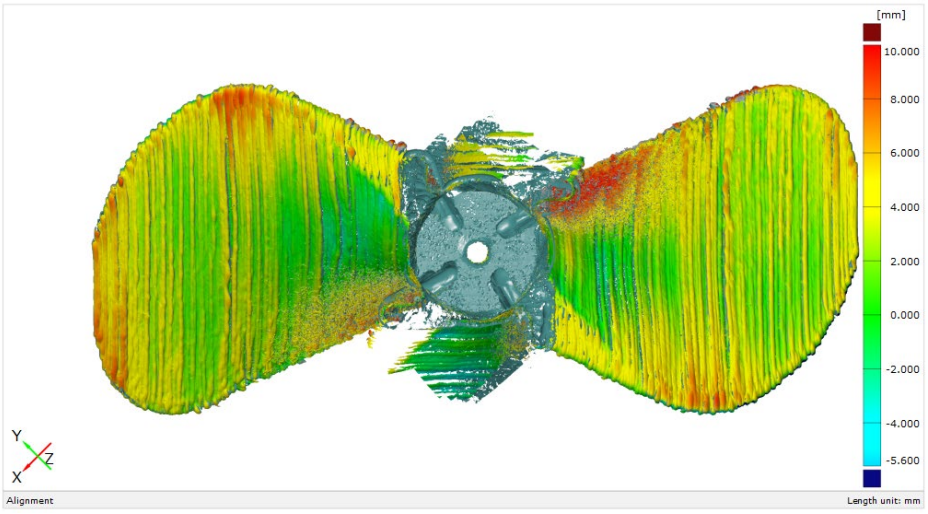

Fig. 9: Bottom view of two opposing blades

The propeller managed to be printed successfully on the first attempt and was scanned by a 3D scanner. Comparisons were done between the as-printed propeller and the input model which was modified and described previously, allowing us to understand the deviation between the actual and intended model. From visual inspection between layers during the printing process, no gaps were noted between contours in the layer, indicating that the adaptive bead width toolpath is capable of properly filling the layer. Two of the blades were scanned and fitted to the input model for comparison, shown in Fig 9 and 10. Looking at the comparison, the scanned part is generally larger than the input model, indicated by green to red regions for most of the print which is desirable to provide allowance for post processing. Underprinting is found mostly on the tip of the blade, suggesting that the blades are shorter than required even though the blades were measured to be taller when probed by the welding torch. This mismatch results in the toolpath from a higher height being utilized during the printing of the blades. With the varying contour, additional overprint and underprint becomes apparent when the contour is shifting quickly, such as the top and bottom tips of the blades. To mitigate this, further calibration can be done on the robotic system to reduce positioning error. Further adjustments can also be made before each stage to adjust the final positioning of each print to the actual position. Such an adjustment can be easily done with the Cartesian coordinate being used.

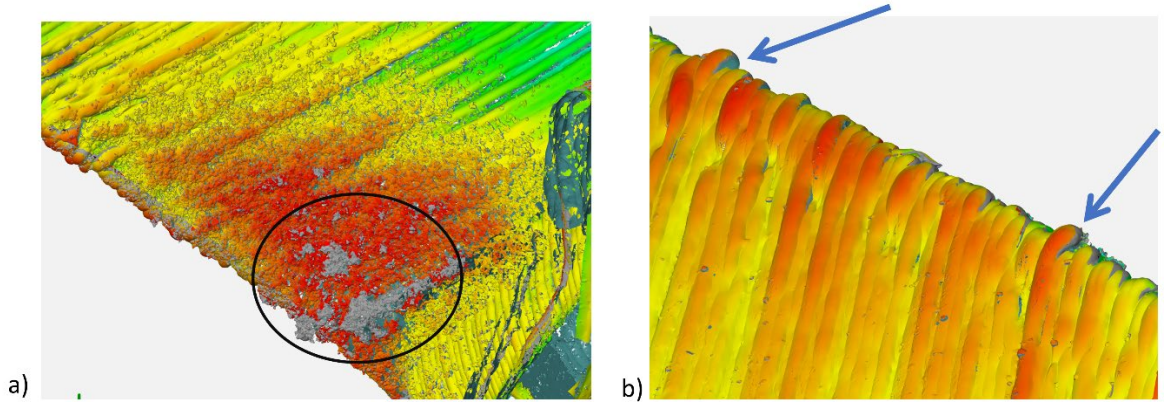

Fig. 10: a) Splatter accumulation in black circle b)Surface waviness at edge of blade with regions where the weld bead is overflowing

Other causes of the dimensional deviations can be attributed to the material and printing process. Splatter is observed to accumulate at a region on the bottom side of the blade, close to the interface at the top of the hub. The splatter thickens the portion of the blade causing overprint in those regions. Such regions of overprint caused by accumulation of splatter are expected and can be excluded from analysis as it is not indicative of the actual dimension. Surface waviness is another contributing factor especially at the tip of the blades where there is overhang and sharp corners. Such conditions result in less stable bead geometry, encouraging the bead to flow outwards causing overprint. Improved toolpath planning methods taking into account of overhang and sharp corners could further improve accuracy.

Conclusion

Multi directional printing with adaptive bead width was shown to be a viable method to print parts with revolved features. By using planar slices, multi directional printing enables the adaptation of variable bead width toolpath with minimal modifications. The approach was applied to print a propeller successfully in the first attempt, demonstrating the viability of the approach. Despite the use of adaptive bead width, further areas of improvement such as handling of overhang and sharp corners have been identified. With multi directional printing approach, such improvements can be developed or adapted from planar printing strategies easily, allowing fast improvement to the process.

References

[1] S. W. Williams, F. Martina, A. C. Addison, J. Ding, G. Pardal and P. Colegrove, "Wire + Arc Additive Manufacturing," *Materials Science and technology,* vol. 32, no. 7, pp. 641-647, 2016.

[2] D. Ding, Z. Pan, D. Cuiuri, H. Li and N. Larkin, "Adaptive path planning for wire-feed additive manufacturing using medial axis transformation," *Journal of Cleaner Production,* vol. 133, pp. 942-952, 2016.

[3] Y. Xiong, S.-I. Park, S. Padmanathan, A. G. Dharmawan, S. Foong, D. W. Rosen and G. S. Soh, "Process planning for adaptive contour parallel toolpath in additive manufacturing with variable bead width," *The International Journal of Advanced Manufacturing Technology,* vol. 105, no. 10, pp. 4159-4170, 2019.

[4] Y. M. Elkhouly, W. S. Lim, A. G. Dharmawan and G. S. Soh, "Adaptive contour based printing of a propeller using hybrid-wire arc additive manufacturing," *Materials Today: Proceedings,* vol. 70, pp. 395-400, 2022.

[5] T. He, S. Yu, Y. Shi and Y. Dai, "High-accuracy and high-performance WAAM propeller manufacture by cylindrical surface slicing method," *The International Journal of Advanced Manufacturing Technology,* vol. 105, pp. 4773-782, 2019.

[6] A. G. Dharmawan and G. S. Soh, "A cylindrical path planning approach for additive manufacturing of revolved components," *Mater Sci Add Manuf,* vol. 1, no. 1, pp. 1-3, 2022.

[7] F. Dai, H. Zhang and R. Li, "Process planning based on cylindrical or conical surfaces for five-axis wire and arc additive manufacturing," *{Rapid Prototyping Journal,* vol. 26, no. 8, pp. 1405-1420, 2020.

[8] R. Wang, H. Zhang, W. Gui-Lan and X. Zhao, "Cylindrical slicing and path planning of propeller in wire and arc additive manufacturing," *Rapid Prototyping Journal,* vol. 26, no. 1, pp. 49-58, 2020.

[9] Y. Ding, R. Dwivedi and R. Kovacevic, "Process planning for 8-axis robotized laser-based direct metal deposition system: a case on building revolved part," *Robotics and Computer-Integrated Manufacturing,* vol. 44, pp. 67-76, 2017.

[10] D. Ding, Z. Pan, D. Cuiuri, H. Li, N. Larkin and S. Van Duin, "Automatic multi-direction slicing algorithms for wire based additive manufacturing," *Robotics and Computer-Integrated Manufacturing,* vol. 37, pp. 139-150, 2016.

[11] K. Lee and H. Jee, "Slicing algorithms for multi-axis 3-D metal printing of overhangs," *Journal of Mechanical Science and Technology,* vol. 29, pp. 5139-5144, 2015.

[12] C. P. Singh, R. Sarma and S. Kapil, "The qualitative analysis of warpage on residual stresses in wire arc additive manufacturing," *Materials Today: Proceedings,* vol. 62, pp. 6619-6627, 2022.